Jpn J Ophthalmol 2004;48:158–162
© Japanese Ophthalmological Society 2004

DOI 10.1007/s10384-003-0034-y

CLINICAL INVESTIGATION

Development of Bilateral, Nonarteritic Anterior Ischemic Optic Neuropathy in an Eye with Diabetic Papillopathy

Tatsuhiko Sato[1], Takashi Fujikado[2], Jun Hosohata[2], Masahito Ohji[2], and Yasuo Tano[2]

[1]Department of Ophthalmology, Social Insurance Kinan General Hospital, Wakayama, Japan; [2]Department of Ophthalmology, Osaka University Medical School, Osaka, Japan

Abstract

Background: Diabetic papillopathy and anterior ischemic optic neuropathy are different clinical entities with different prognoses. We describe a case of diabetic papillopathy that developed into bilateral nonarteritic anterior ischemic optic neuropathy (AION).

Case: A 58-year-old woman with diabetes mellitus had bilateral disc elevation. Goldmann perimetry showed altitudinal hemianopsia in the left eye. The early phase of fluorescein angiography showed hypoperfusion in the superior segment of the left optic disc indicating AION in the left eye.

Observations: During the follow-up period, the visual field of the left eye was further constricted and that of the right eye also developed signs of AION, suggesting that bilateral anterior ischemic optic neuropathy had developed. After steroid pulse therapy, her vision recovered slightly, but the visual field remained constricted in both eyes. The optic discs had a low cup/disc ratio.

Conclusions: Our findings demonstrated that diabetic papillopathy can precede the development of nonarteritic anterior ischemic optic neuropathy. **Jpn J Ophthalmol** 2004;48:158–162 © Japanese Ophthalmological Society 2004

Key Words: anterior ischemic optic neuropathy, diabetic papillopathy, low cup/disc ratio

Introduction

Optic neuropathy in a diabetic patient usually presents either as diabetic papillopathy (DP) or as nonarteritic ischemic optic neuropathy (ION). Generally, DP causes minor visual loss and resolves spontaneously after several months. On the other hand, nonarteritic ION can cause severe visual loss with only limited recovery.

We report a case of DP that developed into bilateral nonarteritic anterior ischemic optic neuropathy (AION).

Received: February 10, 2003 / Accepted: September 20, 2003

Correspondence and reprint requests to: Tatsuhiko Sato, Department of Ophthalmology, Social Insurance Kinan General Hospital, 510 Minato, Tanabe 646-0031, Japan
e-mail: t-satou@kinan-hp.or.jp

Case Report

A 58-year-old woman had noticed blurred vision in her left eye from the first week of August 2001 and consulted an ophthalmologist. She was informed that her optic discs were elevated bilaterally and were surrounded by flame-shaped hemorrhages. On 31 August, she was referred to Osaka University Hospital.

A physical examination showed that she had diabetes mellitus, hypertension, cholesterolemia, and had smoked 20 cigarettes/day for 6 years. She was started on diet therapy for the diabetes mellitus and drug therapy for the hypertension and cholesterolemia.

At the first ophthalmological visit, her best-corrected visual acuity (VA) was 1.5 OU. The critical fusion frequency was 38 Hz in the right and 37 Hz in the left eye. A relative

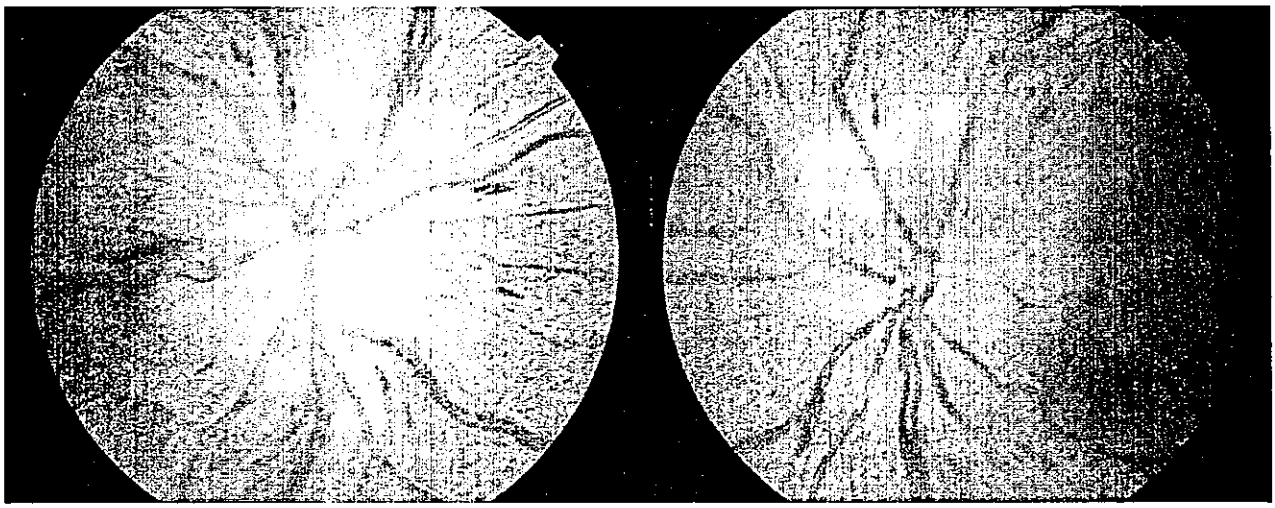

Figure 1. Fundus photograph of the right eye (*left*) and the left eye (*right*) at the first visit of a 58-year-old woman on 31 August 2001. Both optic discs (particularly the superior segment of the left optic disc) were reddish and elevated with blurred margins. The cup/disc ratios were low for both eyes, indicating a so-called disc at risk.

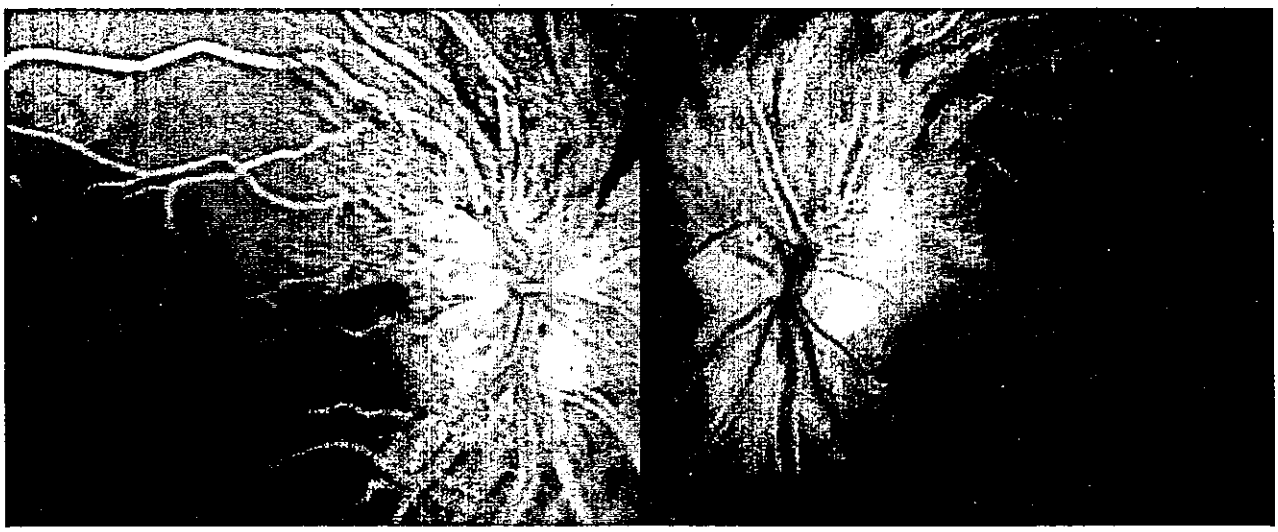

Figure 2. Fluorescein angiography (FA) of the right eye (*left*) and the left eye (*right*) at the first visit. FA showed marked leakage from the right optic disc, hypoperfusion in the superior segment of the left optic disc, and hyperperfusion in the inferior segment of the left optic disc throughout the angiography.

afferent pupillary defect was present in the left eye. Both optic discs were reddish, particularly the superior half of the left disc, and both were elevated with blurred margins. The cup/disc ratios were low for both eyes, indicating a so-called disc at risk (Fig. 1). Fluorescein angiography (FA) showed marked leakage from the right optic disc, hypoperfusion in the superior segment of the left optic disc, and hyperperfusion in the inferior segment of the left optic disc throughout the angiography (Fig. 2). Goldmann perimetry revealed an enlarged blind spot in the right eye and an inferior altitudinal hemianopsia in the left eye (Fig. 3). Diabetic retinopathy was not observed by ophthalmoscopy or FA in either eye.

The blood levels of HbA_{1c} (7.3%–9.5%), glucose (100–400 mg/dl), and total cholesterol (250–300 mg/dl) were higher than normal. Both inflammation and coagulation reactions were normal; for example, the erythrocyte sedimentation rate was 8 mm/h and 25 mm/2 h.

Computed tomography (CT), fat-suppression magnetic resonance imaging (MRI), and magnetic resonance angiography (MRA) results of the head were normal. A carotid echo examination showed extensive plaque formation in the left carotid artery.

Based on these observations and on the results of the ophthalmological examinations, DP in the right eye and nonarteritic AION in the left eye were diagnosed in this

Jpn J Ophthalmol
Vol 48: 158–162, 2004

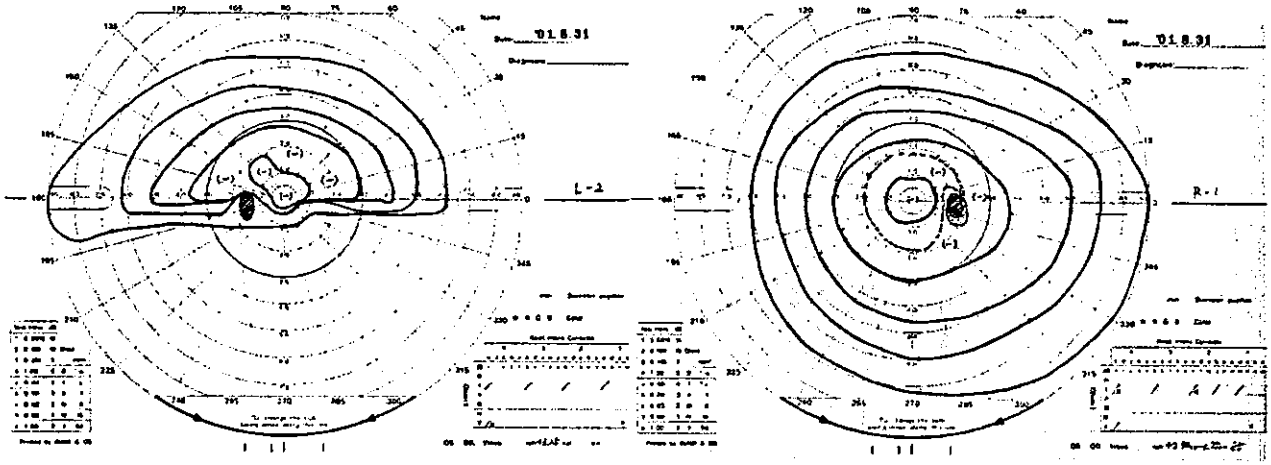

Figure 3. Goldmann perimetry (GP) of the right eye (*right*) and the left eye (*left*) at the first visit. GP revealed an enlarged blind spot in the right eye and inferior altitudinal hemianopsia in the left eye.

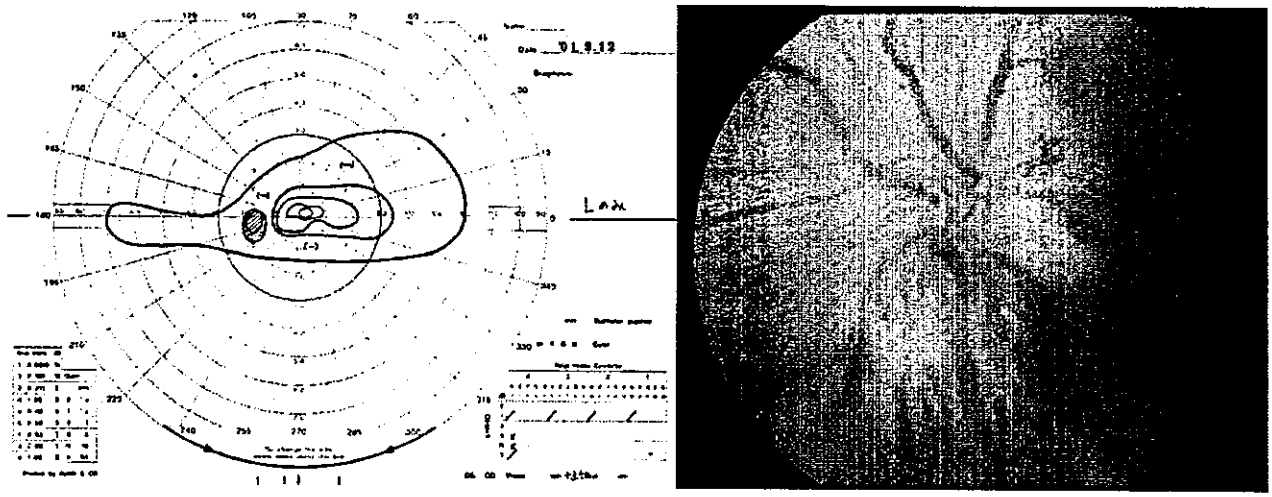

Figure 4. Goldmann perimetry (*left*) and fundus photograph (*right*) of the left eye on 12 September. GP detected a constriction of the upper visual field in conjunction with the inferior altitudinal hemianopsia. The fundus photograph shows a more severe elevation of the optic disc compared with that at the first visit.

patient. She was started on low-dose aspirin therapy (162 mg; Children's Bufferin, 2 tablets/day) from 5 September. On 12 September, VA in her left eye decreased abruptly from 1.0 to 0.1, and a constriction of the upper visual field of the left eye was detected in conjunction with the inferior altitudinal hemianopsia (Fig. 4). Low-dose aspirin therapy was stopped, and she was placed on steroid-pulse therapy (Solu-Medrol, 500 mg/day) for 6 days (from 17 to 19 and 25 to 27 September) under the control of diabetes mellitus by a physician.

In spite of the treatment, VA in her right eye suddenly decreased from 1.0 to 0.1 on 26 September, and the peripheral visual field was markedly constricted (Fig. 5). From 1 October, we resumed low-dose aspirin therapy (81 mg; Children's Bufferin, 1 tablet/day).

On her last visit, on 28 October, her best corrected VA was 0.4 OD and 0.15 OS. Although the elevation of both discs was decreased and the margins of the discs and surrounding areas were clear, the discs were pale and atrophied. In addition, Goldmann perimetry revealed that the peripheral visual field defects were still present in both eyes (Figs. 6A, B).

Discussion

Bilateral disc elevation and a unilateral visual field defect were the initial observations made in this patient. When a patient presents with bilateral optic disc elevation, we must distinguish between nonarteritic AION, arteritic AION, DP, papillitis, papilledema associated with intracranial space occupying lesions, and rhinogenic optic neuropathy. Papilledema and rhinogenic optic neuropathy were ruled out by the results of the CT, fat-suppression MRI, and MRA tests.

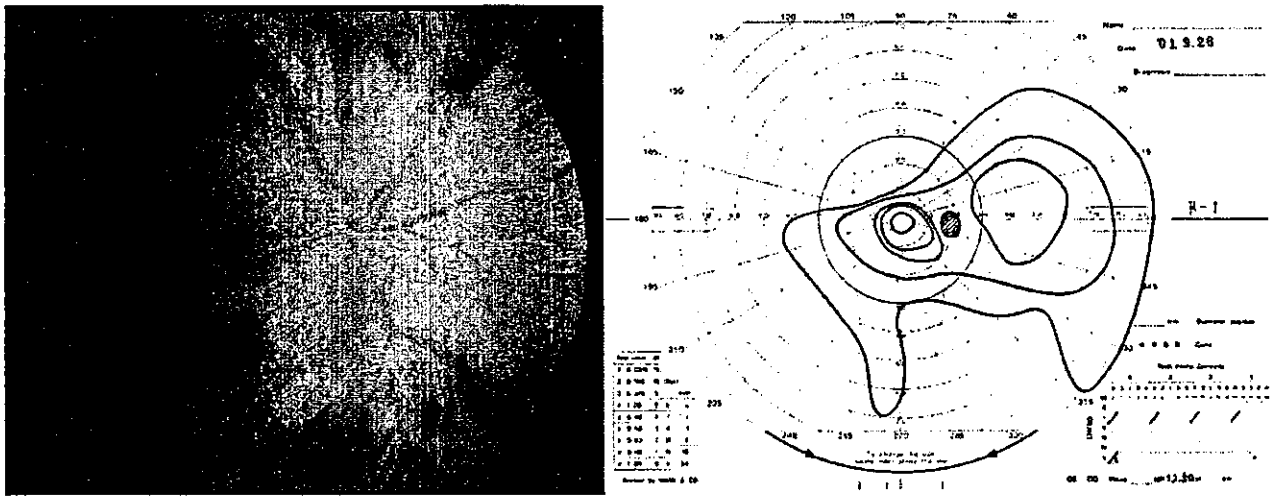

Figure 5. Goldmann perimetry (*right*) and fundus photography (*left*) of the right eye on 26 September. GP detected a marked constriction of the peripheral visual field. The fundus photograph shows a more severe elevation of the optic disc compared with that at the previous visit.

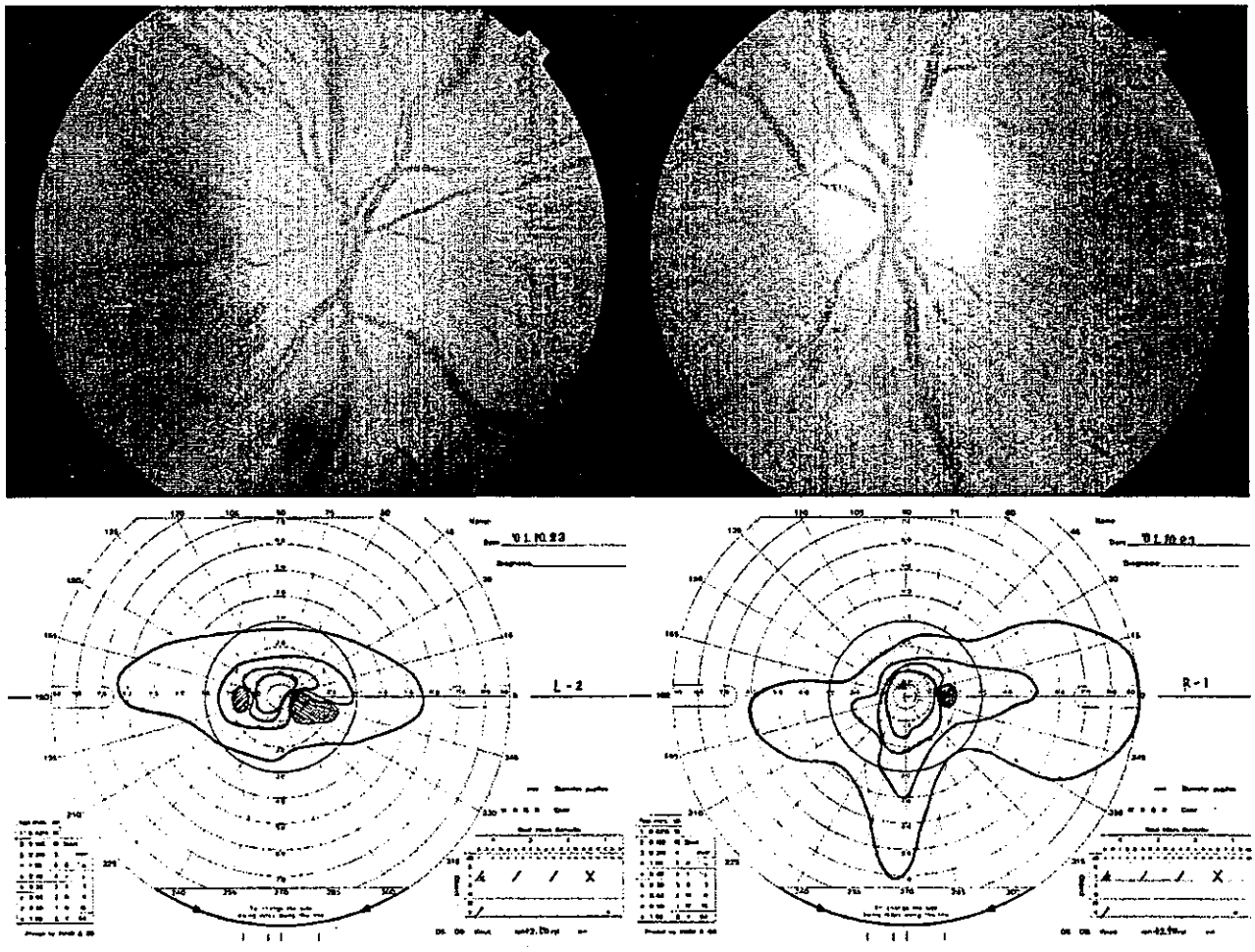

Figure 6. **A** Fundus photograph of the right eye (*left top*) and the left eye (*right top*) on 16 October. Although the elevation of both discs was decreased and the margins of the discs and surrounding areas were clear, the discs were pale and atrophied. **B** Goldmann perimetry of the right eye (*right bottom*) and the left eye (*left bottom*) on 23 October. GP revealed that the peripheral visual field defects were still present in both eyes.

Jpn J Ophthalmol
Vol 48: 158–162, 2004

Several cases of DP have been reported since this condition was originally described by Appen et al. in 1980.[1–4] The features of this condition are tendency to affect patients younger than 40 years of age absence of correlation with the stage of diabetic mellitus or the stage of diabetic retinopathy; no serious disturbance of visual function, such as visual loss or visual field defect; FA shows no delay or staining in the early phase and hyperperfusion from the optic disc and the surrounding areas in the late phase; no remarkable changes in CT images and cerebrospinal fluid; good prognosis; and medication is not necessary because the condition usually resolves spontaneously. Recent reports suggest that DP may be found in older patients with type II diabetes.[5,6]

Nonarteritic AION, on the other hand, has the following features: tendency to occur in patients older than 50 years of age; causes sudden visual loss; is associated with various visual field defects; the optic disc is partially or diffusely pale with intraocular pressure elevation; a characteristic delay of staining in the early phase of FA is coincident with the elevation; no well-established treatment; and prognosis is usually poor.[7]

In our patient, several differences from typical nonarteritic AION were apparent at the first visit; for example, the left optic disc was reddish and elevated and the VA was good. However, we diagnosed our patient as having nonarteritic AION because of the delayed staining in the early phase by FA. Arteritic AION was ruled out because there was no temporal pain, and both inflammation and coagulation reactions were normal.

Several atypical cases of nonarteritic AION have been reported. For example, there is a report that discs are particularly reddish and elevated in eyes with disc at risk.[8] Another report suggests that discs are pale and swollen in arteritic AION and reddish and swollen in nonarteritic AION.[9]

We suggest that the good VA in the left eye at the first visit was because the first attack did not include the papillomacular nerve fiber bundle. However, on 12 September, the patient developed visual loss and a peripheral visual field defect because the second attack did involve the papillomacular fibers.

As far as we know, there are only a few reports of nonarteritic AION in which the visual loss progresses in two stages. Various studies report the frequency of an attack of nonarteritic AION in both eyes, which ranges from 25% to 50%.[10,11] Also the interval between the attacks in the two eyes is reportedly from several days to several years.[10] In our case, the right eye developed AION about 2 months after the first attack in the left eye.

There is no established effective method to treat nonarteritic AION, which differs from arteritic AION. In our case, the patient was hospitalized immediately after the second attack in the left eye. She was given steroid pulse therapy under the control of diabetes mellitus by a physician. Some reports suggest that steroid therapy is effective for visual recovery in eyes with nonarteritic AION.[10,12] Hayreh and Podhajsky stated that in nonarteritic AION, when a branch of the short posterior ciliary artery is blocked, the ischemic edema can compress the surrounding tissues and cause secondary ischemia of the tissues.[12] Therefore, it is reasonable that the VA can be improved by blocking this compression with early steroid therapy.

On the other hand, other researchers have reported that the visual field defects cannot be resolved by steroid therapy.[13] In our case, the VA in the right eye improved by more than two lines (from 0.1 to 0.4), but the visual field remained constricted.

In summary, we have reported a case of DP that developed into bilateral nonarteritic AION. These eyes had a low cup/disc ratio. Although there are recent reports that these two clinical entities are essentially the same disease, with DP being the mildest stage of nonarteritic AION,[14] much is still unknown about the relationship between DP and nonarteritic AION. In all events, it should be remembered that, in diabetic patients having optic disc edema without optic symptoms, DP may precede an attack of nonarteritic AION.[15]

References

1. Lubow M, Makley TA Jr. Pseudopapilledema of juvenile diabetes mellitus. Arch Ophthalmol 1971;85:417–422.
2. Appen RE, Chandra SR, Klein R, Myers FL. Diabetic papillopathy. Am J Ophthalmol 1980;90:203–209.
3. Pavan PR, Aiello LM, Wafai MZ, Briones JC, Cebestyen JG, Bradbury MJ. Optic disc edema in juvenile-onset diabetes. Arch Ophthalmol 1980;98:2193–2195.
4. Barr CC, Glaser JS, Blankenship G. Acute disc swelling in juvenile diabetes: clinical profile and natural history of 12 cases. Arch Ophthalmol 1980;98:2185–2192.
5. Bayraktar Z, Alacali N, Bayraktar S. Diabetic papillopathy in type II diabetic patients. Retina 2002;22:752–758.
6. Regillo CD, Brown GC, Savino PJ, et al. Diabetic papillopathy. Arch Ophthalmol 1995;113:889–895.
7. Ischemic Optic Neuropathy Decompression Trial Study Group. Characteristics of patients with nonarteritic anterior ischemic optic neuropathy eligible for the ischemic optic neuropathy decompression trial. Arch Ophthalmol 1996;114:1366–1374.
8. Kajisa F, Shiroma T, Ogido T, Uehara T, Hayakawa K, Sawaguchi S. Appearance of the optic disc in eyes with anterior ischemic optic neuropathy at Ryukyu University Hospital. Nihon Ganka Kiyo (Folia Ophthalmol Jpn) 2000;51:580–584.
9. Hayreh SS. Anterior ischemic optic neuropathy. II. Fundus on ophthalmoscopy and fluorescein angiography. Br J Ophthalmol 1974;58:964–980.
10. Hayreh SS. Anterior ischemic optic neuropathy. Ganka Rinsho Iho (Jpn J Clin Ophthalmol) 1986;40:581–587.
11. Ellenberger C Jr. Ischemic optic neuropathy as a possible early complication of vascular hypertension. Am J Ophthalmol 1979;88:1045–1051.
12. Hayreh SS, Podhajsky P. Visual field defects in anterior ischemic optic neuropathy. Doc Ophthalmol Proc Ser 1979;19:53–71.
13. Watanabe I, Iijima H, Imai M. Recovery of visual field defects in ischemic optic neuropathy and idiopathic optic neuritis. Nippon Ganka Gakkai Zasshi (Acta Soc Ophthalmol Jpn) 1991;95:986–994.
14. Hayreh SS. Anterior ischemic optic neuropathy. VI. In juvenile diabetics. Ophthalmologica 1981;182:13–28.
15. Hayreh SS. Anterior ischemic optic neuropathy. V. Optic disc edema, an early sign. Arch Ophthalmol 1981;99:1030–1040.

(10)

FOVEAL SENSITIVITY AND FIXATION STABILITY BEFORE AND AFTER MACULAR TRANSLOCATION WITH 360-DEGREE RETINOTOMY

TOMOHITO OYAGI, MD,* TAKASHI FUJIKADO, MD,†‡ JUN HOSOHATA, MD,†‡ MASAHITO OHJI, MD,† MOTOHIRO KAMEI, MD,† KENICHIRO BESSHO, MD,† AND YASUO TANO, MD†

Purpose: To evaluate the functional changes of the fovea by scanning laser ophthalmoscopy (SLO) fundus perimetry after macular translocation with 360-degree retinotomy, and to determine whether the preoperative macular function estimated by the sensitivity of the fovea and the stability of fixation can predict visual acuity after the surgery.

Methods: Macular translocation with 360-degree retinotomy and simultaneous torsional muscle surgery were performed on 25 eyes of 25 patients with choroidal neovascularization. The index of foveal sensitivity (I_{sens}) and the index of fixation stability (I_{fix}) before and after surgery were calculated from the microperimetric data. The preoperative I_{sens} and I_{fix} were compared with postoperative I_{sens} and I_{fix}, respectively. The correlations of preoperative I_{sens} and I_{fix} with the visual acuity after the translocation surgery (VA_{post}) were calculated.

Results: I_{sens} increased in 14 (56%) of 25 eyes. I_{fix} improved in 10 (40%) of 25 eyes. The preoperative I_{sens} and VA_{post} were moderately correlated ($r = -0.434$, $P = 0.0295$), while the preoperative I_{fix} and VA_{post} were highly correlated ($r = 0.530$, $P = 0.0057$).

Conclusion: An increase in foveal sensitivity and an improvement in the fixation stability were demonstrated quantitatively by microperimetry. The preoperative foveal sensitivity and fixation stability were correlated with the postoperative visual acuity. Microperimetry using SLO can be used to investigate foveal function before and after the translocation and to predict the postoperative visual acuity.

RETINA 24:548–555, 2004

Choroidal neovascularization (CNV), occurring mainly in eyes with age-related macular degeneration (ARMD) or with high myopia, is one of the major causes of visual loss especially in industrialized countries.[1] In 1993, Machemer and Steinhorst[2] first reported macular translocation with 360-degree retinotomy, and several modification have been made since then.[3–7] After the fovea is shifted onto healthier retinal pigment epithelium (RPE), the translocated fovea has a normal configuration and function.[8] Thus, macular translocation has the possibility of eliminating the central scotoma and improving visual function.

Before performing the translocation operation, it is very important to know the residual function of the

From the *Department of Ophthalmology, Osaka Rosai Hospital, and the
Departments of †Ophthalmology and
‡Visual Science, Osaka University Medical School, Japan.
The authors have no proprietary interest in any aspect of this study.
Supported by Health Science Grant, Japan.
Reprint requests: Tomohito Oyagi, MD, Department of Ophthalmology, Osaka Rosai Hospital, 1179-3 Nagasone-cho, Sakai-shi, Osaka 591-8025, Japan; e-mail: toyagi@orh.go.jp

Table 1. Data of All Patients

Number	Age, yr	Sex	Operated Eye	Diagnosis	Preop Visual Acuity (VApre)	Postop Best Visual Acuity (VApost)	Preop Sensitivity ($prel_{sens}$)	Postop Sensitivity ($postl_{sens}$)	Preop Fixation ($prel_{fix}$)	Postop Fixation ($postl_{fix}$)
1	79	M	L	ARMD	20/100	20/29	0.60	0.75	11.5	46.5
2	74	M	R	ARMD	20/50	20/40	0.80	0.50	29.9	32.6
3	76	F	L	ARMD	20/67	20/100	0.93	1.00	6.8	7.7
4	71	M	R	ARMD	20/667	20/100	0.61	0.80	23.3	102.6
5	70	F	L	ARMD	20/133	20/50	0.63	1.00	7.4	60.7
6	59	M	L	ARMD	20/67	20/40	0.77	0.40	29.2	14.8
7	78	M	R	ARMD	20/67	20/333	0.40	0.00	41.3	6.7
8	77	F	L	ARMD	20/200	20/222	1.00	0.70	4.5	3.8
9	75	M	L	ARMD	20/100	20/133	0.81	0.70	76.2	29.1
10	75	M	L	ARMD	20/40	20/33	0.83	0.80	6.7	6.9
11	73	F	R	CNV	20/67	20/25	0.63	1.00	4.9	2.5
12	73	M	L	ARMD	20/67	20/67	0.94	0.60	11.4	4.9
13	79	M	L	ARMD	20/400	20/200	0.28	0.60	22.6	30.4
14	66	M	L	ARMD	20/1000	20/500	0.00	0.40	86.3	45.5
15	55	F	R	CNV	20/133	20/50	0.17	0.80	1.6	23.1
16	75	M	R	ARMD	20/200	20/133	0.45	0.45	80.9	80.9
17	68	M	L	ARMD	20/133	20/50	0.63	0.75	12.0	13.1
18	73	M	R	ARMD	20/50	20/133	0.78	0.80	1.4	24.4
19	51	M	R	ARMD	20/500	20/2000	0.15	0.80	75.2	145.6
20	69	F	R	CNV	20/40	20/20	0.75	0.90	2.4	11.0
21	66	F	R	CNV	20/667	20/250	0.27	0.30	22.5	31.0
22	62	F	L	ARMD	20/100	20/133	0.29	1.00	43.0	6.4
23	74	F	L	ARMD	20/133	20/200	0.50	0.20	11.1	39.5
24	72	M	L	Osteoma	20/100	20/100	0.90	1.00	55.3	19.9
25	60	F	R	CNV	20/133	20/29	0.25	0.81	50.0	23.0

ARMD = age-related macular degeneration; CNV = choroidal neovascular membrane.

fovea because preserving or improving foveal function is one of the most important goals to attain after the translocation operation. The location, size, and depth of the central scotoma, and thus the sensitivity of the fovea and the stability of fixation, can be determined quantitatively by using a scanning laser ophthalmoscope (SLO) and fundus perimetry.[9–12] These measures have been used previously to measure the residual function of the sensory retina.[10,13] It has been reported that the use of SLO may help to optimize the selection of patients in cases of limited macular translocation.[14]

The purpose of this study was to obtain a measure of foveal function before and after macular translocation with 360-degree retinotomy. To accomplish this, microperimetry was performed on 25 eyes with CNV before and after a 360-degree macular translocation, and the sensitivity of the fovea was determined from the results of microperimetry. The preoperative sensitivity of the fovea was compared with the postoperative sensitivity. The fixation stability before and after surgery was also determined from the results of microperimetry. We determined whether the residual macular function estimated by foveal sensitivity and the stability of fixation can be used to predict the visual acuity after the 360-degree macular translocation.

Patients and Methods

Fifty-nine eyes of 59 consecutive patients with subfoveal choroidal neovascular membrane caused by ARMD, pathologic myopia, or osteoma underwent macular translocation with 360-degree retinotomy at the Osaka University Hospital from November 1998 to April 2000. Eyes with less than 6 months follow-up and patients who were not examined by microperimetry either a week before or more than 1 month after the surgery were excluded. We also excluded eyes with severe complications during and after the surgery, for example, severe and large damage of retinal pigment epithelium in the fovea or recurrent retinal detachment in the fovea. In the end, 25 eyes of 25 patients (10 women and 15 men) were included in this study (Table 1).

The mean (± SD) age of the 25 patients was 70.0 ± 7.5 years with a range of 51–79 years. The CNV in 19 patients was due to ARMD, in 5 to pathologic myopia, and in 1 to osteoma. The duration of the subjective visual disturbance was less than 6 months in all cases.

The visual acuity before the translocation surgery ranged from 20/1000 to 20/40, and the size of the CNV was less than 3 disk diameters (DD) as measured on the fluorescein angiograms (FA). The duration of the follow-up ranged from 8 to 17 months (12.6 ± 2.5 months).

This research was conducted in accordance with the institutional guidelines of Osaka University and conformed to the tenets of the World Medical Association Declaration of Helsinki. Patient consent was obtained after a thorough discussion of the risks and possible benefits of the surgical treatment.

Surgical Methods

Surgery was performed under local anesthesia by a facial nerve block and retrobulbar injection, or under general anesthesia. In two cases, muscle surgery was performed after the translocation of the fovea. The cyclotorsional surgery included recession of the superior oblique muscle and tucking or advancement of the inferior oblique muscle. In some cases, muscle transposition was also performed on the superior rectus and inferior rectus muscles.

Cataract surgery was performed on phakic patients (20 of 25 cases). The lens was removed by phacoemulsification and aspiration (PEA) or pars plana lensectomy (PPL). For PEA, an intraocular lens (IOL) was inserted into the lens capsule before the vitrectomy, and in the PPL cases, the IOL was placed into the anterior chamber.

Standard three-port vitrectomy was performed with a vitreous cutter. The completion of the posterior vitreous detachment was confirmed with the use of a soft-tipped fluted needle. Intentional bullous retinal detachments were created by injecting BSS-Plus solution (Alcon, Fort Worth, TX) between the retinal pigment epithelium and the sensory retinal layer with a 39-gauge needle at three to five points around the vascular arcade. Fluid-air exchange followed by a slow shaking of the globe was performed to merge the individual bullous retinal detachments. After completion of the retinal detachment, a 360-degree retinotomy was made with a vitreous cutter or vitreous scissors. The retina was rotated superiorly by 10° to 45° around the optic disk and tamponaded by injecting perfluorocarbon onto the retina. Photocoagulation was performed along the edge of the retinotomy after the rotation of the retina. Perfluorocarbon was replaced by silicone oil before closing the three sclerotomy sites.

About 1 month after the translocation operation, the silicone oil in the vitreous cavity was replaced by balanced salt solution. In cases with PPL, an IOL was inserted during the second operation.

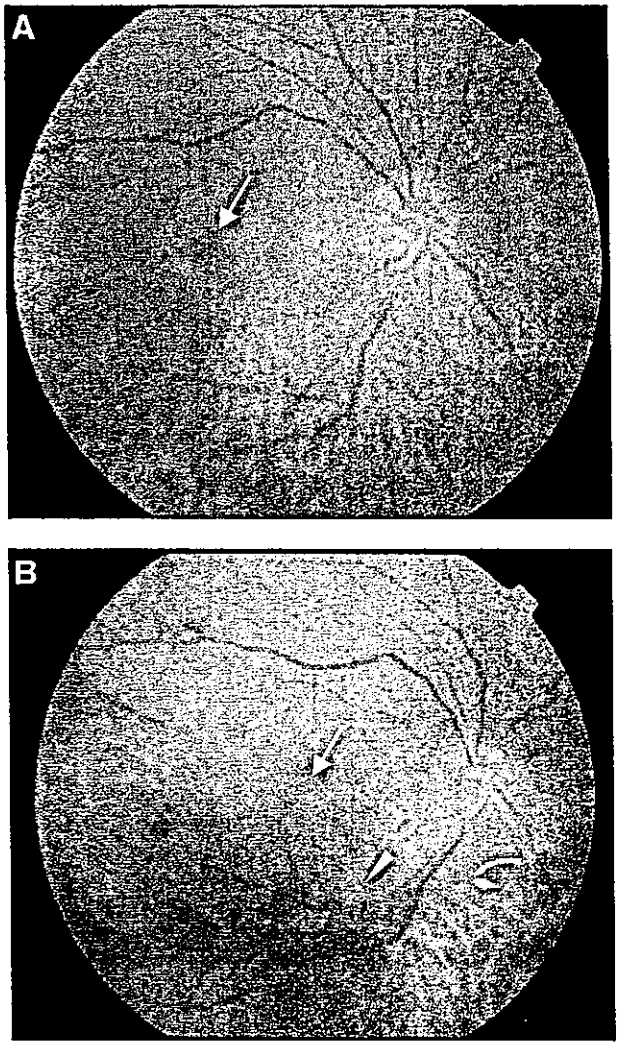

Fig. 1. Preoperative and postoperative fundus photographs of the right eye of Patient 25. **A,** Preoperative fundus photograph shows subretinal choroidal neovascular membrane secondary to myopic neovascular maculopathy under the fovea (arrow). The preoperative visual acuity was 20/133. **B,** Postoperative fundus perimetry shows subretinal choroidal neovascular membrane (arrowhead) located inferior relatively to the fovea (arrow). The postoperative visual acuity was 20/29.

Microperimetry

Microperimetry was performed within a week before and more than 1 month after the translocation surgery with a SLO (Rodenstock Instruments, Germany). Stimulus size was Goldmann III, and stimulus intensity was 10 dB. Stimulus presentation time was 120 ns. Examination time was 15–20 minutes. Number of stimulus points was 100–180. To evaluate the sensitivity and fixation around the fixation point quantitatively, the points tested were distributed around the scotoma and fixation point as homogeneously as possible.

The best-corrected visual acuity was also measured within a week before (VA_{pre}) and at least 1 month

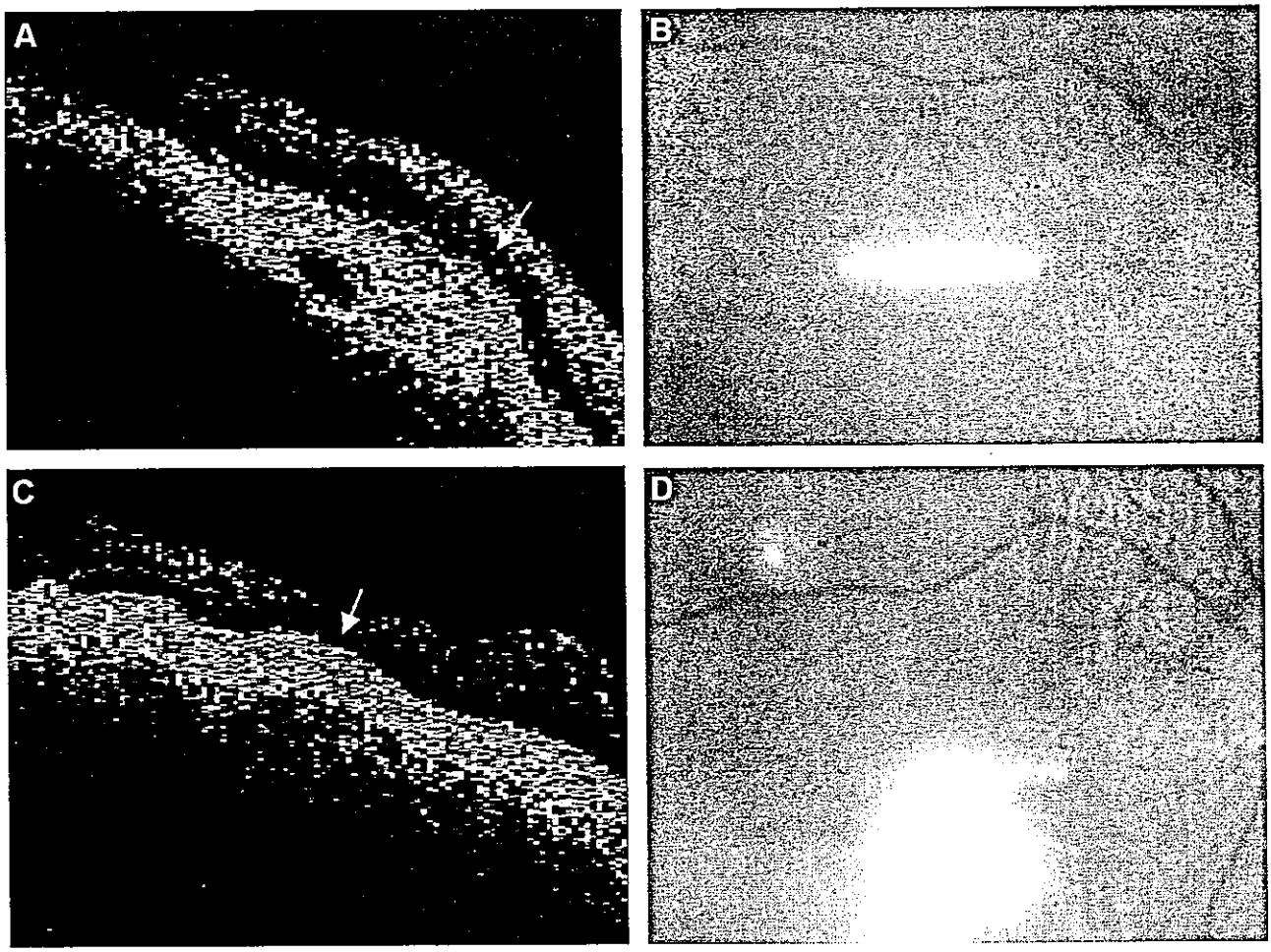

Fig. 2. Preoperative and postoperative optical coherence tomography of the fovea (2.8-mm-long horizontal section) of the right eye of Patient 25. **A,** Preoperative optical coherence tomographic image shows subretinal choroidal neovascular membrane that was secondary to myopic neovascular maculopathy under the fovea (arrow). **B,** Preoperative fundus photograph. White line represents the scan line. **C,** Postoperative optical coherence tomographic image shows almost normal foveal structure and no subretinal choroidal neovascular membrane. **D,** Postoperative fundus photograph. White line represents the scan line.

after the surgery. The best-corrected visual acuity during the follow-up period is expressed as VA_{post}.

The index of foveal sensitivity (I_{sens}) was defined by the number of points with retinal sensitivity divided by the total number of stimulation points within a 1 disk diameter, circular area around the center of the fixation points. I_{sens} was calculated preoperatively and postoperatively as $preI_{sens}$ and $postI_{sens}$, respectively. The $preI_{sens}$ were compared with the $postI_{sens}$.

The index of fixation stability (I_{fix}) was defined as $I_{fix} = (Fx) \times (Fy/DD^2)$, where Fx and Fy are the standard deviations of the fixation points from the center of the fixation point during the examination in the vertical and horizontal directions (arbitrary units), and DD is the length of the long axis of the optic disk. I_{fix} was calculated preoperatively and postoperatively as $preI_{fix}$ and $postI_{fix}$, respectively. The $preI_{fix}$ were compared with the $postI_{fix}$. The correlations of the $preI_{sens}$ and $preI_{fix}$ with VA_{post} were calculated by Pearson's correlation coefficient.

Results

Case Report

A 58-year-old woman with myopia and posterior staphyloma reported that she recently noticed a central blind area in the right eye. Her best-corrected visual acuity was 20/133 in the right eye and 20/30 in the left. The anterior segments were normal except for mild cortical cataracts. Ophthalmoscopy and fundus microscopy of the right eye revealed a subretinal scar with hemorrhage in the fovea (Figure 1A). Optical coherence tomography (OCT) demonstrated a subretinal neovascular membrane (Figure 2A).

Microperimetry with a SLO disclosed a deep scotoma (Figures 3A and 4A). The I_{sens} of the fovea was

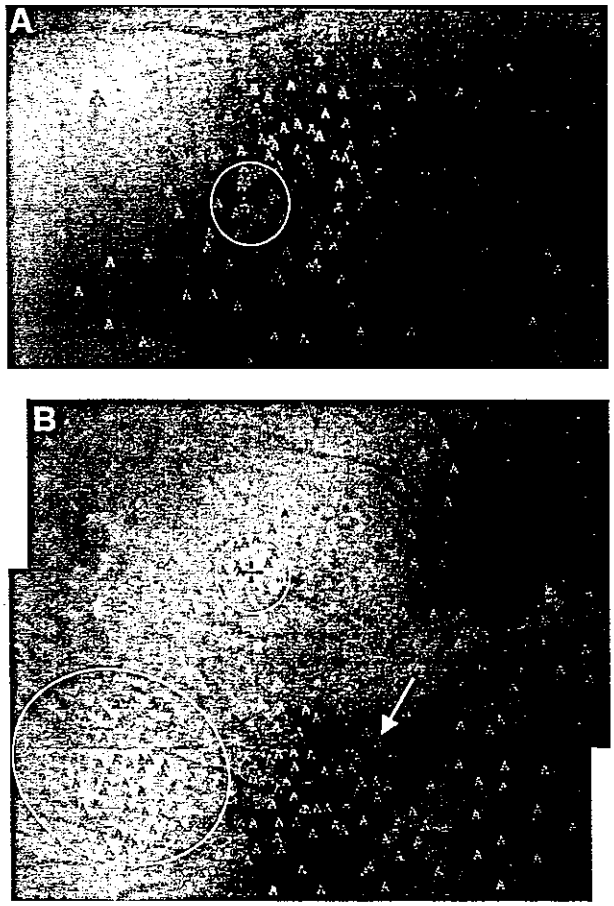

Fig. 3. Preoperative and postoperative microperimetry of the right eye of Patient 25 using scanning laser ophthalmoscope. **A,** Preoperative microperimetry shows a scotoma due to subretinal choroidal neovascular membrane of approximately 1.2 DD with epicenter at the fovea. Preoperative sensitivity of the fovea was 0.25. **B,** Postoperative microperimetry shows that the scotoma in the fovea that was present before the operation was not present after the translocation operation. The scotoma due to the neovascular maculopathy is now located inferior to the new fovea (arrow). Postoperative sensitivity of the fovea was 0.81. Scotoma inferior to the macula was due to the photocoagulation during the translocation operation (yellow circle). The green A's indicate points seen by patient, and the red A's represent points not seen during microperimetry. The blue cross indicates the fixation point. The white circle indicates the circular area around the gravitational center of the fixation points within 1 DD.

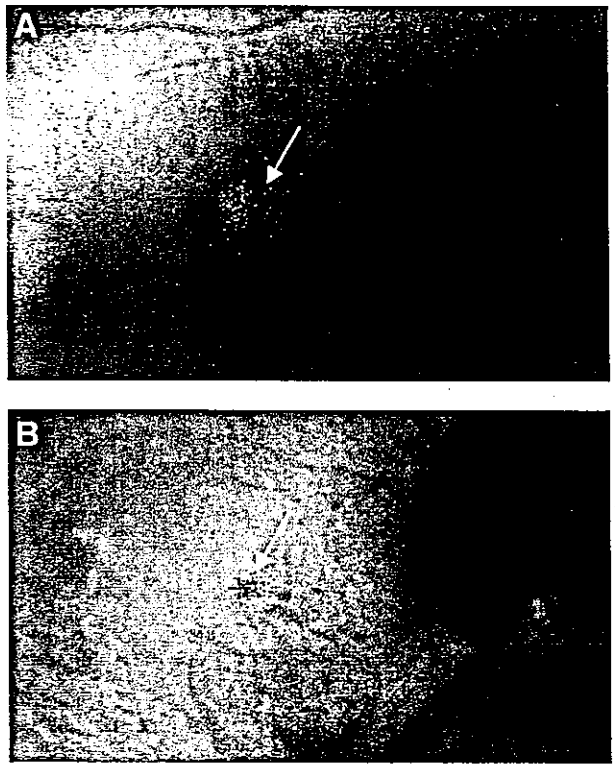

Fig. 4. Preoperative and postoperative fixation map of the right eye of Patient 25 obtained by microperimetry using scanning laser ophthalmoscope. **A,** Preoperative fixation map. Preoperative fixation stability was 50. **B,** Postoperative fixation map. Fixation is improved after the translocation operation. Postoperative fixation stability was 23. The small dot indicates the fixation point (arrow). The blue cross indicates the fixation.

0.25 and I_{fix} was 50 (approximately 1.2 DD in size). Goldmann perimetry (GP) also demonstrated a scotoma within 5 degrees of the fovea (Figure 5A).

After the surgery, the subretinal choroidal neovascular membrane was located inferior to the new fovea (Figure 1B). Postoperative OCT showed that the configuration of the fovea was almost normal (Figure 2C). Microperimetry, 1 month after the surgery, demonstrated an improvement of the foveal sensitivity in the area that formerly covered the subretinal choroidal neovascular membrane (Figure 3B), and fixation was improved (Figure 4B). I_{sens} and I_{fix} were 0.81 and 23 (approximately 0.4 DD), respectively, which indicated that both the sensitivity and fixation had improved after the surgery. GP 1 month postoperatively demonstrated that a scotoma was not present at the new foveal location (Figure 5B). One month after the translocation surgery, the silicone oil was removed. The best-corrected visual acuity after the silicone oil was removed and 3 months after the translocation surgery was 20/29. The patient did not have any visual complaints and reported that the blind spot was no longer present.

Foveal Sensitivity and Fixation Stability

I_{sens} increased more than 5% in 14 eyes (56%), remained unchanged (the change was within 5%) in 3 (12%), and decreased more than 5% in 8 (32%) of 25 eyes. I_{fix} improved (decreased) more than 5% in 10 eyes (40%), remained unchanged (the change was within 5%) in 5 (20%), and worsened (increased) more than 5% in 10 (40%) of 25 eyes.

The VA_{pre} was correlated with VA_{post} (Figure 6; $r = 0.652$, $P = 0.0004$). The postoperative visual

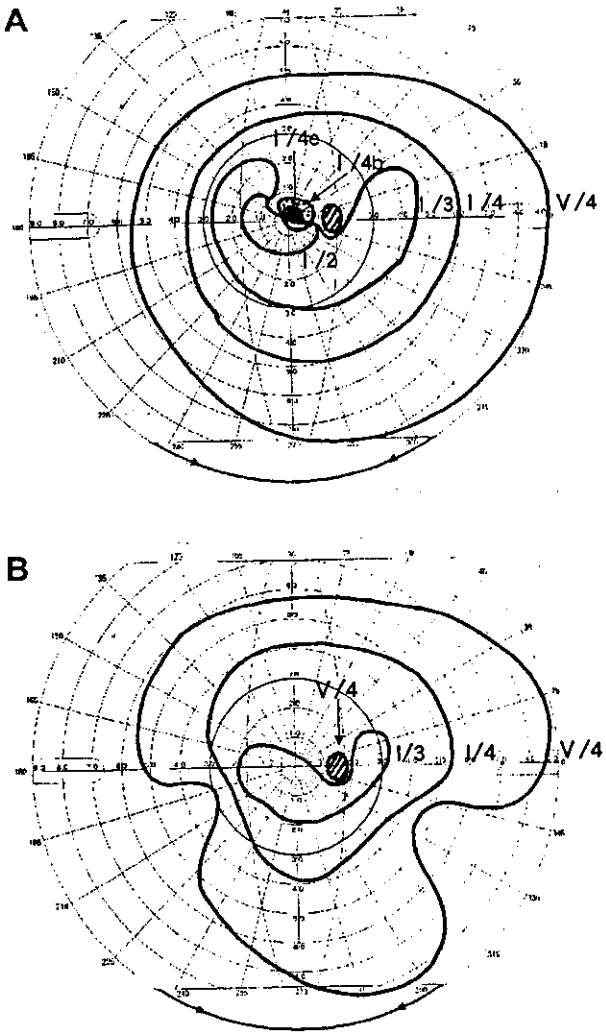

Fig. 5. Preoperative and postoperative Goldmann perimetry. A, Preoperative Goldmann perimetry shows a central scotoma. B, The central scotoma observed before the translocation operation is not present postoperatively.

acuity improved by more than 0.2 logarithm of the minimum angle of resolution (logMAR) units in 10 patients and worsened by more than 0.2 logMAR units in 5 patients.

There was a significant correlation between $preI_{sens}$ and VA_{post} (Figure 7; $r = -0.434$, $P = 0.0295$). The $preI_{fix}$ was also significantly correlated with VA_{post} (Figure 8; $r = 0.530$, $P = 0.0057$). The VA_{post} increased with decreasing $preI_{fix}$.

Discussion

Macular translocation with 360-degree retinotomy is effective for the treatment of CNV because it has the potential of increasing visual acuity and of eliminating the central scotoma. Microperimetry is considered to be one of the most important methods to evaluate the functional effect of the macular translocation operation because it can determine the location, size, and depth of the new scotoma as shown in the case report. Our findings support this, and in most eyes that underwent the macular translocation with 360-degree retinotomy, the scotoma was newly located approximately 30 degrees inferior to the new fovea after the surgery (Figure 3).

SLO was also useful for evaluating the foveal sensitivity and fixation stability.[10] The function of the

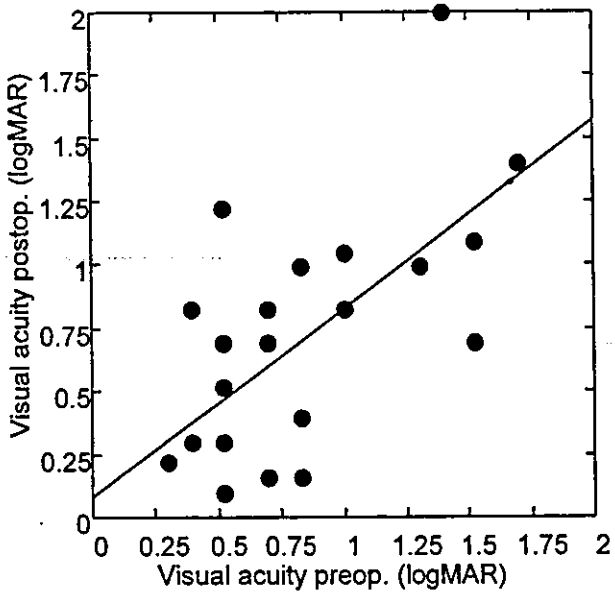

Fig. 6. Correlation between preoperative visual acuity and postoperative best-corrected visual acuity (logMAR units). The linear coefficient of correlation was $r = 0.652$, $P = 0.0004$.

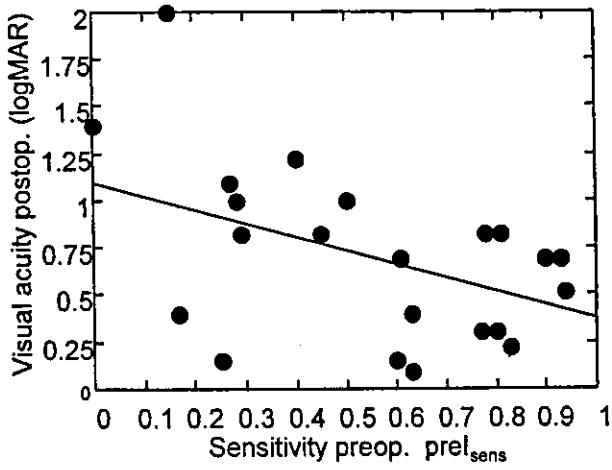

Fig. 7. Correlation between preoperative sensitivity of the fovea and postoperative visual acuity (logMAR units). The linear coefficient of correlation was $r = -0.434$, $P = 0.0295$.

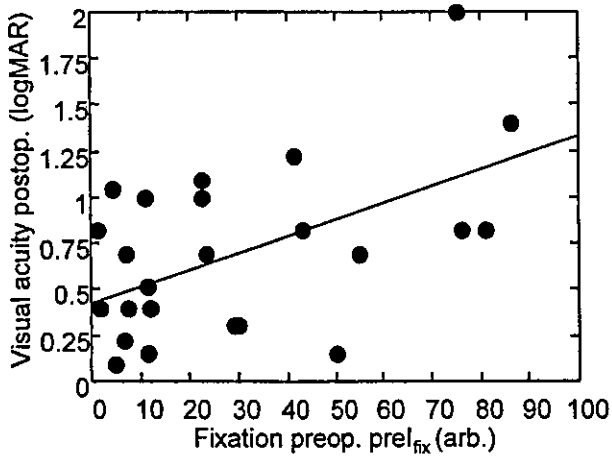

Fig. 8. Correlation between preoperative fixation stability and postoperative visual acuity (logMAR units). The linear coefficient of correlation was r = 0.530, P = 0.0057.

fovea in eyes with macular edema and the effect of laser photocoagulation for macular edema have been assessed by SLO.[13] SLO is also reported to be useful for evaluating foveal function in eyes with idiopathic macula holes,[15,16] with age-related geographic atrophy,[17] and to examine the effects of photocoagulation and surgery for CNV.[18,19] Fujii et al[14] reported that the fixation and microperimetric patterns enabled a better understanding of the macular function in eyes with ARMD, and stated that incorporating these tests may help to optimize patient selection for limited macula translocation. In our study, the preoperative and postoperative sensitivity of the fovea (preI$_{sens}$ and postI$_{sens}$) and preoperative and postoperative fixation stability (preI$_{fix}$ and postI$_{fix}$) were calculated from the data obtained from microperimetry, and these values were statistically treated. By comparing preI$_{sens}$ with postI$_{sens}$, and preI$_{fix}$ with postI$_{fix}$, the efficacy of macular translocation with 360-degree retinotomy for CNV on the sensitivity of the fovea can be evaluated. In addition, the correlation of preI$_{sens}$ and preI$_{fix}$ with the postoperative visual acuity can be evaluated statistically.

I$_{sens}$ increased more than 5% in 14 eyes (56%) and remained unchanged in 3 (12%). I$_{fix}$ improved more than 5% in 10 eyes (40%) and remained unchanged in 5 (20%). The results were most likely due to the translocation of the fovea from the area of the CNV onto healthier pigment epithelium. Foveal function cannot be assessed only by visual acuity especially in cases of macular translocation for CNV, which is designed to decrease the central scotoma. Measurement by microperimetry and the calculation of sensitivity and fixation is an important way to assess the changes in the foveal function. An increase in foveal sensitivity and an improvement in fixation were among the most important factors that result from the translocation, and microperimetry can demonstrate change in the foveal sensitivity and fixation effectively.

VA$_{pre}$ and VA$_{post}$ were strongly correlated (Figure 6), indicating that the postoperative visual acuity can be predicted with some degree of certainty from the preoperative visual acuity. PreI$_{sens}$ and preI$_{fix}$ represent foveal function, and both were also significantly correlated with VA$_{post}$ (Figures 7 and 8). These findings indicate that good VA$_{post}$ would be expected in eyes with high preI$_{sens}$ and low preI$_{fix}$. It has been reported that eyes with stable and central fixation (without dense central scotoma) and good preoperative visual acuity have a greater chance to achieve good vision after limited macular translocation for ARMD.[14] Our results support this, and in addition to preoperative fixation, sensitivity was also found to be important for good postoperative visual acuity.

In conclusion, microperimetric measurements before and after macular translocation with 360-degree retinotomy for CNV are considered to be indispensable from two aspects: for the evaluation of the effect of macular translocation and for the estimation of the postoperative visual acuity. Microperimetry with SLO can determine the preoperative and postoperative foveal sensitivity and fixation in eyes with CNV. The preoperative sensitivities of the fovea and fixation stability were significantly correlated with the postoperative visual acuity in eyes with CNV. We recommend that microperimetry with a SLO be performed preoperatively to obtain these values, which would then allow ophthalmologists to predict the postoperative visual acuity and the potential visual recovery after the macular translocation surgery.

Key words: macular translocation, scanning laser ophthalmoscopy, fixation, foveal sensitivity.

References

1. Ryan SJ, Hinton DR, Murata T. Choroidal Neovascularization. In: Ryan SJ, Ogden TE, Hinton DR, Schachat AP, Wilkinson CP, eds. Retina. 3rd Ed. Vol. 2 St. Louis: C.V. Mosby, 2001;1003–1023.
2. Machemer R, Steinhorst UH. Retinal separation, retinotomy, and macular relocation: Part II. A surgical approach for age-related macular degeneration? Graefes Arch Clin Exp Ophthalmol 1993;231:635–641.
3. de Juan E Jr, Loewenstein A, Bressler NM, Alexander J. Translocation of the retina for management of subfoveal choroidal neovascularization: Part II. A preliminary report in humans. Am J Ophthalmol 1998;125:635–646.
4. Ninomiya Y, Lewis JM, Hasegawa T, Tano Y. Retinotomy and foveal translocation for surgical management of subfo-

veal choroidal neovascular membranes. Am J Ophthalmol 1996;122:613–621.
5. Eckardt C, Eckardt U, Conrad HG. Macular rotation with and without counter-rotation of the globe in patients with age-related macular degeneration. Graefes Arch Clin Exp Ophthalmol 1999;237:313–325.
6. Kamei M, Roth DB, Lewis H. Macular translocation using scleral clips to create an outpouching radial fold of the sclera, choroid and retinal pigment epithelium: ARVO abstracts. Invest Ophthalmol Vis Sci 2000;41(Suppl):S540.
7. Au Eong KG, Pieramici DJ, Fujii GY, et al. Macular translocation: unifying concepts, terminology, and classification. Am J Ophthalmol 2001;131:244–253.
8. Fujikado T, Ohji M, Kusaka S, et al. Visual function after foveal translocation with 360-degree retinotomy and simultaneous torsional muscle surgery in patients with myopic neovascular maculopathy. Am J Ophthalmol 2001;131:101–110.
9. Fujikado T, Ohji M, Hosohata J, Hayashi A, Oda K, Tano Y. Comparison of visual function after foveal translocation with 360 degrees retinotomy and with scleral shortening in a patient with bilateral myopic neovascular maculopathy. Am J Ophthalmol 2000;130:525–527.
10. Fujikado T, Ohji M, Saito Y, Hayashi A, Tano Y. Visual function after foveal translocation with scleral shortening in patients with myopic neovascular maculopathy. Am J Ophthalmol 1998;125:647–656.
11. Rohrschneider K, Becker M, Schumacher N, Fendrich T, Volcker HE. Normal values for fundus perimetry with the scanning laser ophthalmoscope. Am J Ophthalmol 1998;126:52–58.
12. Rohrschneider K, Becker M, Kruse FE, Fendrich T, Volcker HE. Stability of fixation: results of fundus-controlled examination using the scanning laser ophthalmoscope. Ger J Ophthalmol 1995;4:197–202.
13. Rohrschneider K, Bultmann S, Gluck R, Kruse FE, Fendrich T, Volcker HE. Scanning laser ophthalmoscope fundus perimetry before and after laser photocoagulation for clinically significant diabetic macular edema. Am J Ophthalmol 2000;129:27–32.
14. Fujii GY, de Juan E Jr, Sunness J, Humayun MS, Pieramici DJ, Chang TS. Patient selection for macular translocation surgery using the scanning laser ophthalmoscope. Ophthalmology 2002;109:1737–1744.
15. Sjaarda RN, Frank DA, Glaser BM, Thompson JT, Murphy RP. Assessment of vision in idiopathic macular holes with macular microperimetry using the scanning laser ophthalmoscope. Ophthalmology 1993;100:1513–1518.
16. Nakabayashi M, Fujikado T, Ohji M, Saito Y, Tano Y. Fixation patterns of idiopathic macular holes after vitreous surgery. Retina 2000;20:170–175.
17. Sunness JS, Bressler NM, Maguire MG. Scanning laser ophthalmoscopic analysis of the pattern of visual loss in age-related geographic atrophy of the macula. Am J Ophthalmol 1995;119:143–151.
18. Rohrschneider K, Gluck R, Becker M, et al. Scanning laser fundus perimetry before laser photocoagulation of well defined choroidal neovascularisation. Br J Ophthalmol 1997;81:568–573.
19. Loewenstein A, Sunness JS, Bressler NM, Marsh MJ, de Juan E Jr. Scanning laser ophthalmoscope fundus perimetry after surgery for choroidal neovascularization. Am J Ophthalmol 1998;125:657–665.

DTD 5

Available online at www.sciencedirect.com
SCIENCE DIRECT®

Sensors and Actuators A xxx (2004) xxx–xxx

SENSORS AND ACTUATORS A PHYSICAL

www.elsevier.com/locate/sna

Micro-sized photo-detecting stimulator array for retinal prosthesis by distributed sensor network approach

Akihiro Uehara*, Yi-Li Pan, Keiichiro Kagawa, Takashi Tokuda, Jun Ohta, Masahiro Nunoshita

Graduate School of Materials Science, Nara Institute of Science and Technology, 8-1-1 Takayama, Ikoma, Nara 630-0101, Japan

Received 12 July 2004; received in revised form 21 September 2004; accepted 13 November 2004

Abstract

In this paper, we propose a flexible retinal prosthetic device using a distributed sensor network. The novel point of the proposed device is that the flexible stimulator consists of micro-sized CMOS devices linked in a network. In the micro-sized CMOS device single-wire serial interface, a photosensor with a pixel-level analog-to-digital converter (ADC), an image processing circuit, and a current driver circuit are integrated. The device is fabricated using 0.6 μm CMOS technology with a size of 500 μm × 500 μm. We present the results of a successful test of a prototype device.

Keywords: Retinal prosthesis; Implantable electrode; Distributed sensor network; Pixel-level ADC

1. Introduction

Retinal prosthetic devices have attracted a great deal of attention for potential application in the partial recovery of human vision [1–3]. In the basic concept of retinal prosthesis, two-dimensional phosphene, induced by the patterned electrical stimulation of retinal tissue with degenerated photoreceptors, is expected to be a substitute for image perception [3–4]. Intra-ocular retinal prosthetic devices are promising in that they can convert a projected image on the retina into an electrical stimulus pattern. We have been developing vision-chip-based photo-detecting retinal prosthetic devices and systems with the aim of a realizing retinal prosthesis with hundreds of stimulus points for the recovery of clear vision [5–8].

Conventional retinal prosthetic devices are classified into two categories according to the stimulus electrode used: (1) a polyimide-based flexible micro-machined electrode array and (2) a monolithic, silicon-based microelectronic electrode array. For the first category [9–13], ASICs (consisting of a wireless interface circuit, analog multiplexers, and current drivers) have been developed to control the stimulus current of the flexible electrode array [15–16]. In this approach, however, the number of stimulus points is limited by the maximum number of I/O pads, which makes it difficult to achieve thousands of stimulus points. For the second category [5–7,17–20], the implantation of thinned devices on retinal tissue has been proposed and demonstrated. Hundreds of stimulus points can be achieved by this approach, although the brittleness of thin silicon devices makes them unsuitable for long-term implantation in terms of reliability [8].

In this paper, we propose a new intra-ocular retinal prosthetic device in the stimulus electrodes using a distributed sensor network approach, and discuss the micro-sized stimulator—the key device for the proposed intra-ocular retinal prosthetic device [14]. Our aim is to realize a flexible device with a thousand stimulus points. The proposed device shown in Fig. 1 is an array of micro-sized photo-detecting stimulators fixed on a flexible and biocompatible printed circuit board (PCB). The optical image on the retina is transformed into a 2D electrical stimulus pattern by micro-sized

* Corresponding author. Tel.: +81 743726054; fax: +81 743726052.
E-mail address: u-akihir@ms.aist-nara.ac.jp (A. Uehara).

0924-4247/$ – see front matter © 2004 Elsevier B.V. All rights reserved.
doi:10.1016/j.sna.2004.11.023

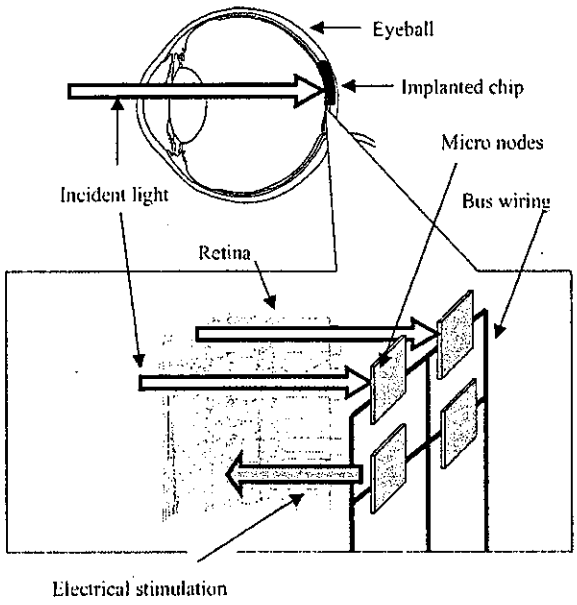

Fig. 1. Concept of retinal prosthetic device.

devices implanted under the retinal tissue. We call the micro-sized photo-detecting stimulator device a 'micronode'.

The proposed retinal prosthetic device has the following advantages over conventional devices: (1) the device is flexible and can bend along the curvature of an eyeball, thus allowing the stimulus electrodes to closely touch the retinal tissue closely; (2) high-density, large, flexible retinal prosthetic devices are possible; (3) the system is simple because a camera and an image processing unit are not required outside the eye.

We had three concerns in the circuit design: (1) minimizing the device size by using a single-wire interface circuit; (2) ensuring low power consumption suitable for a wireless power supply; (3) converting the incident light pattern into an electrical stimulus pattern by using a photosensor circuit with image signal processing. In this paper we discuss these design issues for the micronode. We also present measurement results of a prototype micronode, fabricated using 0.6 μm CMOS technology.

This paper is organized into four sections. In Section 2, we discuss the system architecture, functionality, and circuit design issues. The measurement results and demonstrations of the chip are presented in Section 3. Section 4 summarizes device performance and offers possible methods and means of improvement, followed by Section 5, the conclusion.

2. The intra-ocular retinal prosthetic device by distributed sensor network

Advantages of the proposed intra-ocular retinal prosthetic device over conventional devices are clearly shown in Fig. 2: (1) the maximum number of stimulus electrodes is not restricted by the maximum number of the I/O pads and (2) natural perception is given by direct conversion from the retinal projected image to the spatial electrical stimulus pattern.

Conventional intra-ocular retinal prosthetic devices have a serious problem in that the maximum number of I/O pads or connection wires restricts the maximum number of stimulus electrodes. It is because the stimulus electrodes are directly connected to the telemetry chip by wires, as shown in Fig. 2(a). On the other hand, in the proposed device depicted in Fig. 2(b), the conventional micro-machined stimulus electrodes have been replaced with micro-sized CMOS devices that consist of an on-chip electrode, a serial interface circuit, and a photosensor. Because each micronode is linked through the single-wire serial bus, the restriction of the number of the stimulus electrodes is resolved.

Furthermore, the proposed device converts the retinal projected image into the pixelized spatial stimulation pattern when each micronode implanted under the retina stimulates the retina if the detecting light intensity at the micronode location is larger than a threshold value.

2.1. Design issues of the micronode—device size and power consumption

In order to restore clear perception, the micronode size is determined to be 500 μm square by the spatial resolution of phosphene, as reported in Refs. [21,22]. The number of serial bus wires is fixed at two in order to minimize the circuit area because a wire bonding pad occupies a rather large circuit area, about 100 μm square. A minimum number of serial bus wires is also preferable in order to incorporate the micronode on a cost-effective single-side PCB.

Since the electrical power of intra-ocular devices is derived from electromagnetic coupling, the safe exposure of the human body to rf energy restricts the average power consumption of intra-ocular devices [9–12] to tens of milliwatts. The power consumption of our device is given by

$$P_{\text{total}} = N_{\text{node}} P_{\text{node}}, \quad (1)$$

where N_{node} is the number of micronodes that the device has and P_{node} the power consumption of a micronode. Therefore, the average power dissipation of a micronode without electrical stimulation power should be smaller than 10 μW to achieve a 1000 stimulus points.

To realize both small circuit area and low power consumption, we designed the serial bus signal modulation to send both data and clock signals so that the micronode has no internal oscillator, which usually requires a large circuit area as well as a lot of power. We also designed a simple serial bus protocol that makes the control logic circuit of the micronode small.

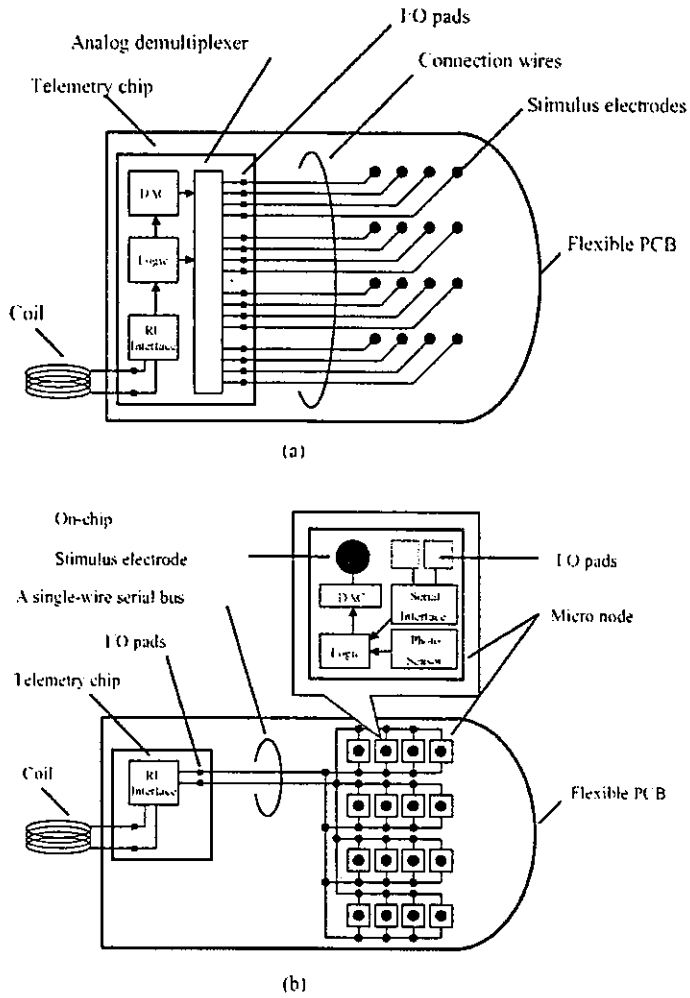

Fig. 2. Diagrams of intra-ocular retina prosthetic devices. (a) Conventional device with a telemetry ASIC fixed on a flexible PCB with a stimulus electrode array. (b) Proposed device with network-linked micronodes to control stimulus current.

2.2. Bus protocol and operation sequence of micronode

The micronode stimulates the retina with square current pulses when the incident light intensity is larger than a threshold value, where the threshold value and the stimulus pulse parameters (amplitude and pulse widths) are set by the serial bus.

Pulse width modulation (PWM) is used for bus signal modulation, as shown in Fig. 3(a), because a delay circuit that occupies small circuit area can recover the clock and data. The bits 1 and 0 are modulated into 1 and 15 μs low pulses, respectively. The bit rate is 50 kbit/s since the symbol time interval is 20 μs. Data is recovered by sampling the bus signal using the clock signal that rises after 10 μs from the falling edge of the bus signal. To suppress the power consumption, the micronode uses the recovered clock signal as its internal clock signal and has no internal oscillator, which usually requires a lot of power.

The data sequence shown in Fig. 3(b) is based on indivisual packets consisting of an 8-bit address field followed by an 8-bit data field. Packets with any address values other than 0xff are called configuration-mode packets, and a packet with an address value of 0xff is an imaging-mode packet. Each micronode has unique 8-bit address value from 0x01 to 0xfe, thus 254 micronodes can be connected to a serial bus. The data field value of the configuration-mode packet is set in the stimulus current amplitude data register of the micronode that is specified by the address field value of the packet. The configuration-mode packet/imaging-mode packet grouping activates the micronode that is addressed by the correlating configuration-mode packet to start photo-detection and electrical stimulation.

The stimulus pulse timing and threshold value of photo binarization are given by the time intervals of six pulses following the imaging-mode packet, as shown in Fig. 3(b). Because of this technique, we can achieve a small circuit area while maintaining a wide range of timing, as the micronode does not require a timing circuit.

The threshold value of photo binarization is controlled through the time interval t_2 as shown in Fig. 3(b). Assuming

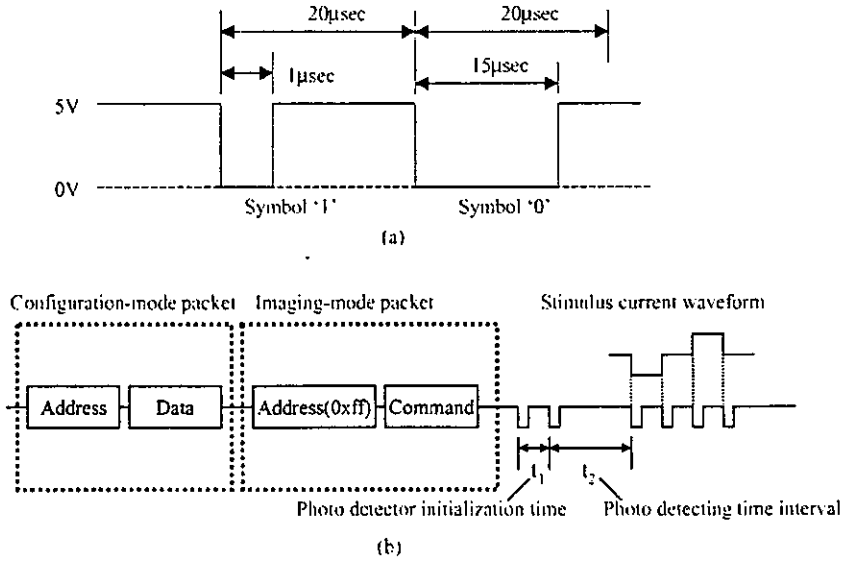

Fig. 3. Serial bus waveforms. (a) Bit encoding by pulse width modulation. (b) Bus signal sequence for photo-detection and successive electrical stimulation.

that the light intensity is uniform during the time interval t_2, the integration value of the incident light is given by

$$S_{\text{det}} = K_{\text{p}} \int_0^{t_2} L \mathrm{d}t = K_{\text{p}} L t_2 \tag{2}$$

where L is the incident light intensity and K_{p} the photosensor sensitivity. The micronode outputs stimulus pulses when the value S_{det} is larger than the internal fixed value S_{th}. In other words, the following condition is met:

$$L \geq \frac{S_{\text{th}}}{K_{\text{p}} t_2}. \tag{3}$$

Therefore, we can control the threshold value by the time interval t_2.

2.3. Circuit design

A block diagram of a micronode is shown in Fig. 4. A micronode consists of an MOS diode, an off-chip capacitor, a current reference circuit, a single-wire serial interface, a photosensor, and a current driver circuit. The serial interface circuit recovers data and clock signals from the PWM bus signal and the finite state machine (FSM) decodes the packet data from the recovered signals. The current driver outputs square current stimulus pulses when the incident light intensity to the photosensor is larger than the threshold value.

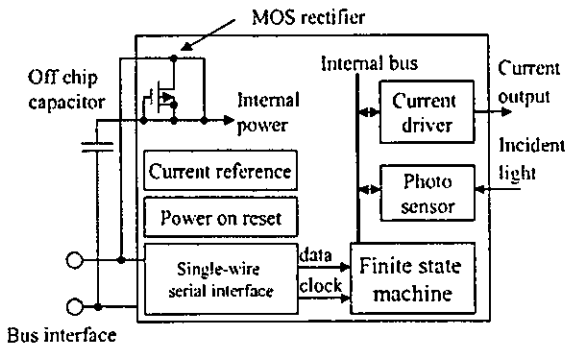

Fig. 4. Block diagram of micronode.

For power reduction, we designed a reference current circuit with extremely small output current to reduce bias currents of the serial interface circuit. We also considered power control so that the FSM activates the current driver and photosensor only when they are needed.

For circuit size reduction, we designed the reference current circuit with only MOSFETs, because the resistance requires a large circuit area. We also designed the pulse–frequency–modulation (PFM) photosensor, which is a digital read-out pixel sensor within a small circuit area.

2.3.1. MOS diode and off-chip capacitor

The arrangements of the MOS diode and the off-chip capacitor are shown in Fig. 4. When the bus line is pulled high by the telemetry chip, the diode in the half-wave rectifier turns on and charges the capacitor. The stored charge provides power to the internal circuits of the micronode when the telemetry chip pulls the bus line low to transmit data.

A p-channel MOSFET is used for the MOS diode because a MOS diode composed of an n-channel MOSFET shows a rather large forward voltage drop due to the body effect. The n-well of a p-channel MOSFET is tied to the internal supply voltage to avoid reverse current through parasitic p–n junction diodes between the n-well and the source or drain.

The off-chip capacitance value must be large enough to supply energy to the internal circuit when the bus signal is

low. The minimum off-chip capacitance value is given by

$$C_{pwr} = \frac{I_{sup} t_{low}}{V_{dd} - V_{min}}, \quad (4)$$

where I_{sup} is the maximum current dissipation including the stimulus current, t_{low} the bus low pulse duration, V_{dd} the internal operational voltage when the bus is pulled high, and V_{min} the minimum operational voltage. Because the off-hip capacitance value inversely proportional to the minimum operating voltage V_{min}, the minimum operating voltage should be as low as possible to use a micro-sized off-chip capacitor. The peak current consumption of the micronode is 320 μA and the longest bus low pulse duration is 15 μs, and thus the micro-sized off-chip capacitance of 3300 pF can be used when the bus high voltage and minimum operating voltages are 5 and 2 V, respectively.

2.3.2. *Reference current circuit*

A reference current source is necessary as a bias current source of the delay circuit in a serial interface circuit and also as the reference current of a digital-to-analog converter (DAC). A micro-power current reference circuit without resistance [26] is designed for supply voltages as low as 2 V because the supply voltage drops during data transmission. The output reference current is 100 nA with a supply current of 1.5 μA. General current references are derived from voltage references by means of an additional voltage-to-current converter, which requires a resistance. Because a large circuit area is necessary for the resistance, to design the general current reference circuit with 100 nA output current, only MOSFETs are used in the reference current circuit where the resistors are replaced with the MOSFETs.

Fig. 5 is a simplified schematic of the reference current circuit with transistor *W/L* ratios. The source voltage of M11, if M5 and M6 are in weak inversion, is given by

$$V_{sd11} = U_T \ln\left(\frac{S_{M5} S_{M2}}{S_{M6} S_{M1}}\right), \quad (5)$$

where U_T (=kT/q) is the thermal voltage and S_{M5}, S_{M2}, S_{M6}, and S_{M1} are the *W/L* ratios of the respective MOSFETs. With the transistor geometry ratios shown in Fig. 5, the source voltage of M5 is 44 mV at room temperature. This results in a bias current of 100 nA with gate geometries of M11, M5, M3, and M1 of *W/L* are 8/200, 480/1, 30/0.6, and 4/60, respectively.

2.3.3. *Serial interface circuit*

The serial interface circuit recovers data and clock signals from the PWM bus signal. In the PWM waveform, the falling edge represents the clock, and the pulse duration encodes a bit. The data and clock are recovered by two-state processing. First, the clock signal is recovered from the bus signal by means of the bus signal falling edge detection. Second, the data is recovered from the PWM bus signal by sampling the bus signal at the falling edge of the recovered clock signal. The clock signal falls after 10 μs from the bus signal falling edge. This allows the use of simple demodulator circuits as described below.

The serial interface circuit shown in Fig. 6 consists of a current source, capacitor, and a voltage comparator. The delay time is given by the charging time of the capacitor *C*1 of 420 fF with a bias current of 50 nA of the transistor M2. *C*1 starts to charge when the reset transistor M7 is turned off and M4 is turned on at the falling edge of the bus signal. The node voltage of capacitor *C*1 is compared with the reference voltage (about 0.8 V) generated by the reference voltage source, which consists of transistors M5 and M6 with a bias current of 50 nA given by the transistor M3. The supply current of the comparator is designed to be 150 nA for low power consumption.

The design challenges of the serial interface circuit are low power consumption and a wide operating supply voltage range. To suppress current dissipation, an extremely small bias current I_b supplied by the current reference circuit is used as the bias current of the delay circuit and comparator. Although the delay time varies from device to device due to bias current dispersion from device mismatch between M1 and M2, the data can be recovered correctly since the ratio of

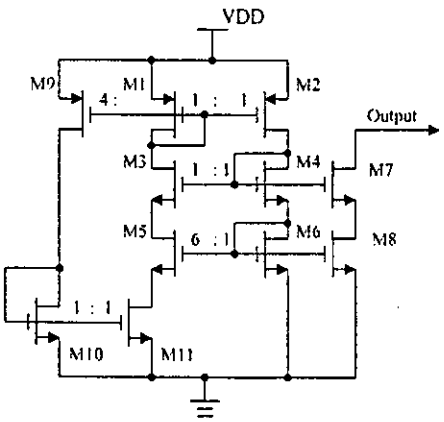

Fig. 5. Schematic of reference current circuit with transistor geometry ratios.

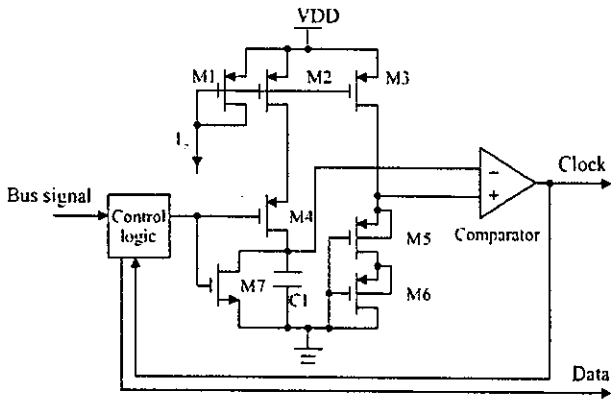

Fig. 6. Schematic diagram of serial interface circuit.

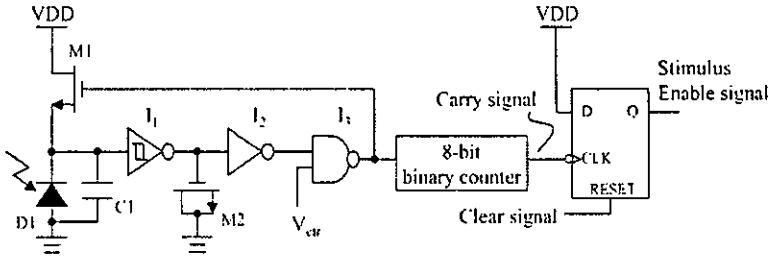

Fig. 7. Circuit schematic of PFM photosensor circuit and image binarization circuit.

the pulse duration between the symbols '1' and '0' is designed to be large, with a value of 15.

2.3.4. Photosensor circuit with pixel-level ADC and image processing

Fig. 7 is a circuit diagram of a pixel-level analog-to-digital converter (ADC) photosensor circuit [23–25] and an image processing circuit. The photosensor circuit consists of two circuit blocks, a light-to-frequency converter photosensor, and an image signal binarization circuit. Image processing is essential for a retinal prosthesis in order to construct a perceivable image from raw image data [19].

A PFM photosensor (consisting of a photodiode D1, reset transistor M1, Schmidt trigger I_1, and logic inverters) operates as a ring oscillator in which the output frequency of the sensor is given by

$$f_{\text{out}} = K_{\text{p}} L, \tag{6}$$

where K_{p} is the sensitivity of the PFM photosensor, and L the incident light intensity [6]. The operation of the PFM photosensor circuit is described in Ref. [6]. The PFM photosensor is activated through the control signal V_{ctr} only during the photo-detection period to suppress excess power dissipation. A parasitic diode between the n-well and p-substrate with geometry of 15 μm × 15 μm is used as a photodiode for its high sensitivity and small dark current.

The image binarization circuit is an 8-bit binary counter with a D flip-flop. Stimulus current output is enabled in the case where the counter overflows during the detecting time t_2, as shown in Fig. 3(b). In other words, stimulus is enabled when the PFM photosensor outputs more than 256 pulses during the detecting time t_2. The threshold light intensity for stimulation is given by Eq. (3), where S_{th} is 256.

2.3.5. Current driver circuit with current DAC

Fig. 8 is the current driver schematic. The stimulus driver circuit employs a 4-bit NMOS binary-weighted current-mode DAC to produce the biphasic currents with 2-bit full-scale current amplitudes of 64, 128, and 256 μA. The amplitude value is configured by the configuration-mode packet as described previously. The stimulus current amplitude is given by

$$I_{\text{stim}} = 64\,\mu\text{A}\,\text{D}[6:5]\frac{\text{D}[3:0]}{16}, \tag{7}$$

where I_{stim} is the stimulus current amplitude, D[6:5] the 2-bit full-scale stimulus amplitude value, and D[3:0] the 4-bit amplitude value. The full-scale stimulus current amplitude is controlled by switching the number of output buffers from one to four through the 2-bit value. The 4-bit amplitude value is input to the binary-weighted DAC, which consists of 15 transistors. The current driver circuit is disabled during the non-stimulating period to suppress power consumption by keeping the gate potential of the transistor M2 to GND.

The stimulus pulse timing is controlled by setting the gate potential of switch transistors, shown in the dash-lined box (Fig. 8), to either power supply voltage (VDD) or GND. When

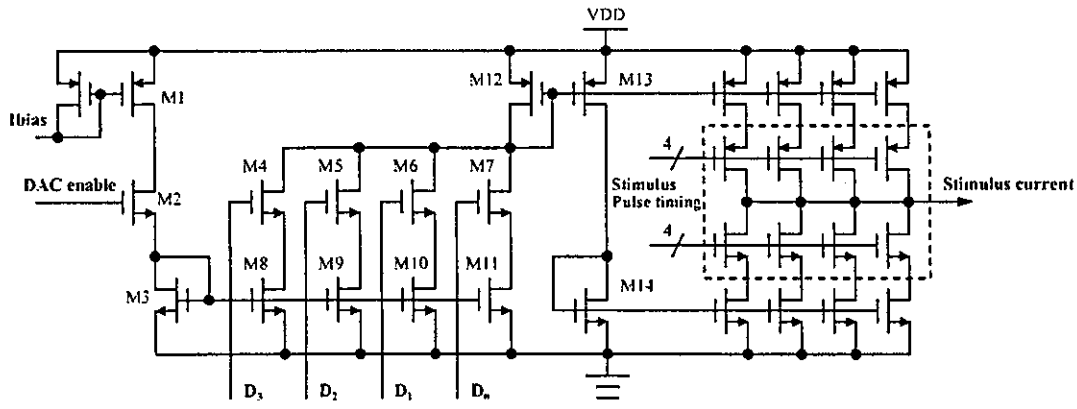

Fig. 8. Circuit diagram of current driver circuit including 4-bit DAC and bias circuit.

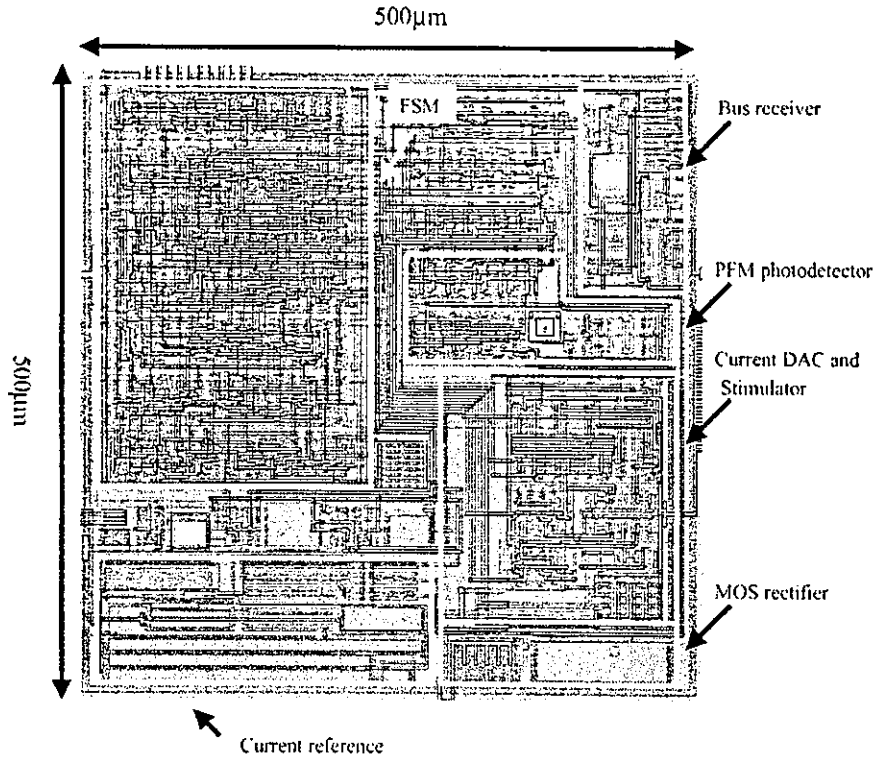

Fig. 9. Device microphotograph.

the gate potential of the p-channel and n-channel MOSFETs are GND, anodic current flows from the stimulus electrode to the reference. Cathodic current flows when the gate potential of the p- and n-channel MOSFETs is VDD. To prevent unexpected stimulus current flow during the non-stimulating duration, the stimulus electrode is kept to high impedance by setting the gate potentials of the p- and n-channel MOSFETs to VDD and GND, respectively.

3. Measurement results

Fig. 9 is a micrograph of the micronode. A prototype device was fabricated using AMS 0.6 μm CMOS technology. The circuit size of the micronodes was 500 μm × 500 μm, except for the bonding pads. The micronode device area is occupied by the FSM (27%), serial interface circuit (6%), PFM pixel circuit and 8-bit binary counter (9%), stimulus circuit (11%), and current reference circuit (11%).

3.1. Reference current circuit

The reference current measured as a function of supply voltage is shown in Fig. 10. The results show that the circuit operating voltage is in the range from 2 to 5 V with an output resistance as large as 900 MΩ. The output resistance is large enough to keep the current deviation under 5 nA within the supply voltage range. The measured average current and current deviation in 15 circuits are 130 nA and 9.7 nA, respectively.

Although a fairly large spread in current values of about ±30% was obtained as expected from a Monte Carlo simulation, the spread did not affect device operation. The serial interface circuit operated correctly even under a large current deviation because the ratio of the low pulse width was large, with a value of 15. Clearly a stimulus current, proportionate to the reference current, does not cause a problem because the external control device sets the stimulus current amplitude by the configuration-mode packet. Temperature dependence of the reference current also should not significantly affect the circuit, since the chip temperature is kept close to body temperature in the eyeball.

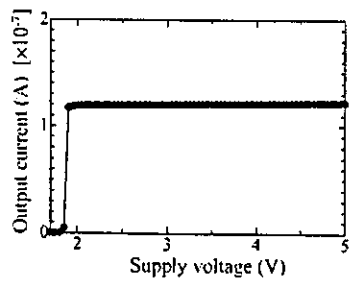

Fig. 10. Experimental results of reference current circuit characteristics.